ELSEVIER

Contents lists available at ScienceDirect

Additive Manufacturing

journal homepage: www.elsevier.com/locate/addma



Mechanical anisotropy in polymer composites produced by material extrusion additive manufacturing



Nadim S. Hmeidat^a, Robert C. Pack^b, Samantha J. Talley^c, Robert B. Moore^c, Brett G. Compton^{a,b,*}

- ^a Mechanical, Aerospace, and Biomedical Engineering Department, University of Tennessee, Knoxville, TN 37996, USA
- ^b Material Science and Engineering Department, University of Tennessee, Knoxville, TN 37996, USA
- ^c Department of Chemistry, Macromolecules Innovation Institute, MII, Virginia Tech, Blacksburg, VA 24061, USA

ARTICLE INFO

Keywords: Additive manufacturing Extrusion Direct ink writing Anisotropy Polymer composites

ABSTRACT

Extrusion-based additive manufacturing technologies, such as direct ink writing of filled polymer resins, have shown a great potential for the development of printed components with superior structural and functional properties. However, the associated extrusion process induces preferred orientation on high-aspect-ratio filler materials as they extrude through the deposition nozzle, causing strong mechanical anisotropy in printed components. Printing-induced anisotropy is a critical issue that complicates the straightforward design of additively manufactured components. The goal of this work is to gain a better understanding of the anisotropy in printed polymer composites by investigating the effects of filler morphology and print parameters on the mechanical properties of printed composites. Inks are formulated using fumed silica particles or nanoclay platelets as the primary viscosifying agent, and silicon carbide (SiC) whiskers as the primary mechanical reinforcement. Mechanical anisotropy is characterized via 3pt-flexural tests for epoxy ink formulations utilizing fumed silica or nanoclay, with or without SiC whiskers, and printed at three different print speeds, using three different nozzle sizes. Orientation of nanoclay is also characterized using small- and wide-angle x-ray scattering. Results show that smaller nozzle diameters and higher deposition rates lead to greater anisotropy when nanoclay or SiC fillers are utilized, while the use of fumed silica alone results in mechanical behavior that is independent of print parameters and print path. Superior flexure strength values up to 215 MPa are obtained with SiC whiskerreinforced composites when tested parallel to the print direction.

1. Introduction

Additive manufacturing (AM) of polymer composites is a rapidly growing area, as researchers seek to improve strength, stiffness, and functionality of printed components over existing AM technologies that predominantly utilize unfilled polymers. Material extrusion AM, in particular, has been a major focus in AM of polymer composites, in part because the extrusion process is amenable to deposition of highly filled, high viscosity resins [1–6]. In addition, extrusion processes are effective at aligning and orienting high-aspect-ratio filler materials in the direction of extrusion [7–13]. This feature enables more effective reinforcement from the filler materials [4,14–20], and, coupled with the ability to select different print paths for each layer in a component, provides unique opportunities to design composite layups into the printed part [21]. In general, this deposition-related alignment of filler materials manifests as anisotropy in strength and stiffness relative to

the print direction [4,5,22]. However, anisotropy in transport [17,23,24] and thermal [25] properties have also been reported.

To manipulate filler orientation and enable greater control over anisotropy in printed materials, new deposition techniques have been developed. For example, Raney and Compton, et al. demonstrated a rotating print head that imparts a helical fiber arrangement with spatial control over the helical angle through modulation of rotation rate [26]. Kokkinis et al. demonstrated spatial control over filler orientation in printed composites by utilizing an external magnetic field and magnetized platelet fillers [27]. Collino et al. utilized acoustic focusing within a deposition channel to concentrate, align, and arrange a wide range of fillers within printed filaments [28,29]. Gladman et al. utilized carefully designed print paths in conjunction with a material that undergoes anisotropic swelling (as a result of filler alignment) to print actuating structures with elegantly programmed deformation modes [30]. Despite these exciting demonstrations of controlling filler orientation to

^{*} Corresponding author at: Mechanical, Aerospace, and Biomedical Engineering Department, University of Tennessee, Knoxville, TN 37996, USA. E-mail address: brettcompton@utk.edu (B.G. Compton).

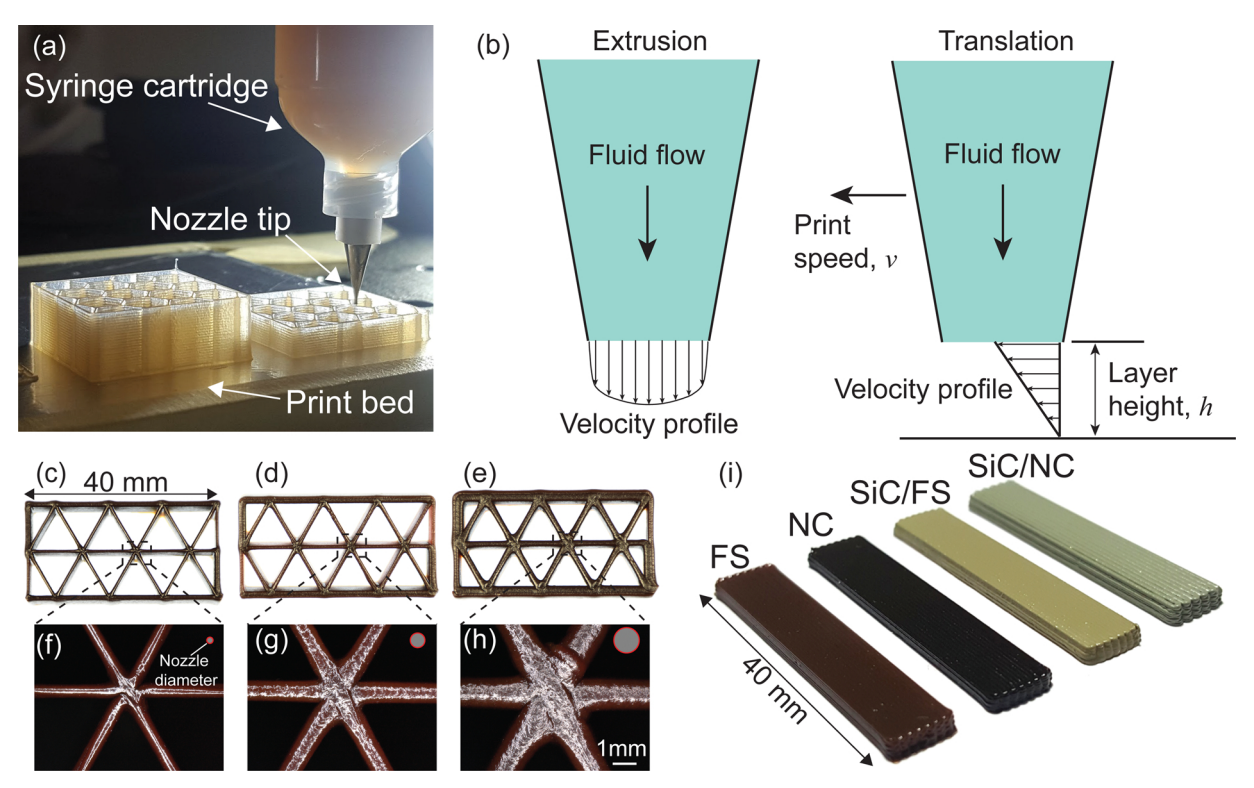


Fig. 1. (a) Direct ink writing (DIW) process using a 410-μm-diameter nozzle (b) Cartoon depicting the approximate velocity profiles that result from extrusion and translation during printing. (c – e) Photographs of triangular honeycombs printed with nozzle sizes of (c) 233 μm, (d) 609 μm and (e) 1041 μm. (f – h) Optical micrographs showing print features as a function of nozzle diameter. (i) Rectangular mechanical test specimens composed of fumed silica (FS), nanoclay (NC), SiC/FS and SiC/NC, printed with a 609-μm-diameter nozzle. Only longitudinal specimens are shown.

achieve prescribed mechanical or functional anisotropy, there have been few basic experimental studies investigating the fundamental relationships between print parameters, filler morphology, and anisotropy in 3D-printed composite materials.

Orientation of non-spherical particles in a flowing fluid has been studied for nearly a century. For example, in Jeffrey's analysis of dilute ellipsoidal particles immersed in a viscous fluid [31], he calculated how oblate (plate-like) and prolate (rod-like) spheroids will reorient in both simple shear and extensional flows. In the limit of an infinitely thin disc or an infinitely slender rod, particles are predicted to adopt a stable orientation with their long dimension aligned in the direction of flow for either type of flow. However, particles with finite thickness are predicted to continue to rotate in simple shear flows, in what are now called Jeffrey orbitals. Conversely, for purely extensional flows even finite-sized particles are predicted to adopt stable orientation along the direction of extension [32]. The periodic motion of particles in flowing fluid has been observed experimentally in dilute and concentrated suspensions [32,33], and very recently in numerical simulations of highly confined flows of concentrated fibers in non-Newtonian fluids wherein each particle is explicitly resolved [20]. Many authors have extended Jeffrey's analysis and applied it to the rheology of short fiber suspensions and to predict the fiber orientation in short fiber composites made via extrusion and injection molding, among others. Notably, Folgar and Tucker developed a modified model that included a fiberfiber interaction term to enable prediction of the orientation distribution function for short fibers in concentrated suspensions [32], and Advani and Tucker introduced the use of orientation tensors to approximate the fiber orientation distribution function and enable efficient numerical calculation of the evolution of fiber orientation through various flow scenarios [34].

A significant result of these types of analyses is that fiber orientation for extrusion processes is expected to be predominantly dictated by the total amount of extensional strain that is applied to the extrudate,

which is set by the draw ratio or area reduction ratio [10], the ratio of the diameter of the fluid reservoir to that of the extrusion die. Experimental studies, however, are somewhat less conclusive. For example, while Goettler identified a strong correlation between measured fiber orientation and the area reduction ratio in glass fiber-reinforced epoxy resins, he also noted a slight dependence on rate of elongational strain, which he attributed to porosity in the mixture [10,35]. Farkash and Brandon [8] studied orientation of SiC whiskers in a ceramic slurry subject to extrusion and identified a strong correlation between fiber orientation and the length of the extrusion die (with the diameter held constant), and they too noted a mild dependence of fiber orientation on extrusion rate [8]. Peng et al., in one of the first demonstrations of material extrusion AM of epoxy composites, observed a significant increase in the alignment of glass fibers along the print direction with an increase in draw ratio [19], which they achieved by increasing the translation speed of the print head while keeping the flow rate of the material constant. Interestingly, they did not note any difference in fiber orientation between a 1.6-mm-diameter deposition nozzle and a 0.6-mm-diameter nozzle, when flow rate and translation speed were held constant, but they did note an increase in orientation with increase in flow rate while keeping constant the translate speed of the print head. They attributed this observation to "plowing of the material surface" by the nozzle [19], reminiscent of using a doctor blade to cast a tape of material.

Observations of particle orientation as a result of tape casting processes have also led to mixed conclusions. For example, Watanabe et al. [36] studied tape casting of bismuth titanate platelets and found no correlation between platelet orientation and shear rate, but did observe an increase in platelet orientation with platelet concentration in the suspension [36]. On the other hand, Wu and Messing [37] observed strong correlation between shear rate in a tape casting process and the orientation of SiC whiskers in an acrylate-based suspension of mullite particles and SiC whiskers. Finally, Galgali et al. [38] investigated the

effect of shear rate on orientation of nanoclay particles in polypropylene subject to a tape casting process and found no correlation between shear rate and particle orientation when the nanoclay had not been compatibilized with the polypropylene, but they observed greater orientation of particles with increasing shear rate for clay that had been compatibilized to the polymer matrix. Because the material extrusion AM process utilizes highly concentrated suspensions with particles that may or may not be functionalized to interact with the carrier fluid, and because the printing process includes aspects of both traditional extrusion and tape casting (Fig. 1b), it would appear worthwhile to study particle orientation effects in AM processes in greater depth.

To that end, the overarching goal of the present work is to a gain a deeper understanding of the phenomena that govern anisotropy in polymer composites printed via material extrusion AM. To do so, we utilize filler materials with different morphologies to develop viscoelastic epoxy-based inks for direct ink writing (DIW) (Fig. 1a). Filler materials include fumed silica (FS) particles, nanoclay (NC) platelets, and silicon carbide (SiC) whiskers, and were chosen because they are frequently used to reinforce polymer resins, impart favorable printing behavior to epoxy resins, and because they span the range of morphology from oblate (NC) to spherical (FS) to prolate (SiC) (Fig. 2). Furthermore, because mechanical anisotropy is frequently observed in material extrusion AM of unfilled polymers [39,40], use of the FS is expected to provide a baseline measure of anisotropy that is not expected to be related to particle orientation. Using inks containing these fillers, rectangular mechanical test specimens are printed using different nozzle sizes and print speeds, and mechanical properties are measured in 3pt-flexural tests, with test specimens printed using print paths oriented along the length of the beam (longitudinal specimens) and transverse to the length of the beam (transverse specimens) (Fig. S1). Print patterns, microstructure, and filler alignment are studied using cross polarized light microscopy, small- and wide-angle x-ray scattering, and scanning electron microscopy (SEM). Through this work, we aim to elucidate the effects that nozzle size and print speed have on the strength and stiffness of printed polymer composites comprised of isotropic and anisotropic filler materials. Insights gained from this work will enable more robust design of 3D-printed composite parts.

2. Experimental

2.1. Materials

Epon 826 epoxy resin (Momentive Specialty Chemicals, Inc., Columbus, OH) was utilized as the DIW ink base. Basionics VS 03, 1-Ethyl-3-methylimidazolium dicyanamide (EMIM DCA) ionic liquid (Sigma-Aldrich, Inc., St. Louis, MO) served as the curing agent. Three different filler materials were utilized to impart mechanical

reinforcement and favorable rheology for 3D printing: i) Cab-o-sil TS-720 fumed-silica (FS) (Cabot Corporation, Alpharetta, GA), ii) Garamite 7305 nanoclay (NC) platelets (BYK-Chemie GmbH,

Wesel, Germany), and iii) SF-1E epoxy-functionalized silicon carbide (SiC) whiskers (Haydale Technologies Inc, Greer, SC) (Fig. 2). The properties of ink constituents are listed in Table 1.

2.2. Formulation

All inks were mixed using a centrifugal planetary mixer (FlackTek, Inc., Landrum, SC). Ink batches were prepared using 20 g of epoxy resin and 1 g of the curing agent, mixed together at 1700 rpm for 60 s. Filler materials were then added in specific increments and mixed under vacuum at 0.1 atm. All ink compositions are summarized in Table 2. For the FS ink, the total amount of FS was added in two increments, each followed by mixing for 60 s at 1700 rpm. Finally, the sides of the mixing container were scraped using a spatula and the final mixture was mixed for another 60 s at 1800 rpm. The NC ink was prepared following the same steps as in [5]. The SiC-based inks were prepared as follows: SiCwhiskers were added and mixed at 1800 rpm for 180 s, then 1.7 g (5.07 wt.%) of NC (or FS) was added to serve as a rheology modifier, followed by mixing for 120 s at 2000 rpm. Finally, the sides of the container were scraped, and the mixture was mixed for an additional 120 s at 2000 rpm. All mixing steps were carried out under vacuum at 0.1 atm. Mixtures with single-filler material were also formulated to investigate the effects of individual filler morphology on the rheological properties of an epoxy resin (Fig. S2). It was not possible to formulate a printable ink using SiC whiskers alone.

2.3. Ink rheology

Rheological properties of the ink were measured using a Discovery HR-2 Rheometer (TA Instruments, New Castle, DE) with 25 mm parallel platens for all ink formulations and 40 mm parallel platens for the unfilled epoxy resin. The apparent viscosity was measured using continuous flow sweeps at controlled shear rates from 0.01 to 30 s $^{-1}$. The storage (G') and loss (G'') moduli were measured using an oscillatory stress sweep in stress control mode at a frequency of 1 Hz. All measurements were preceded by a conditioning step comprised of continuous shear at 0.01 s $^{-1}$ applied for 120 s, followed by a rest period for 120 s. Measurements were conducted at ambient temperature (\sim 21 °C). A gap of 500 μ m was used for all formulations except SiC/NC, which used a gap of 1000 μ m.

2.4. 3D-printing and curing schedule

Test samples were printed using a 3-axis gantry (Shopbot Tools, Inc. Durham, NC) equipped with solenoid valves and air pressure regulator

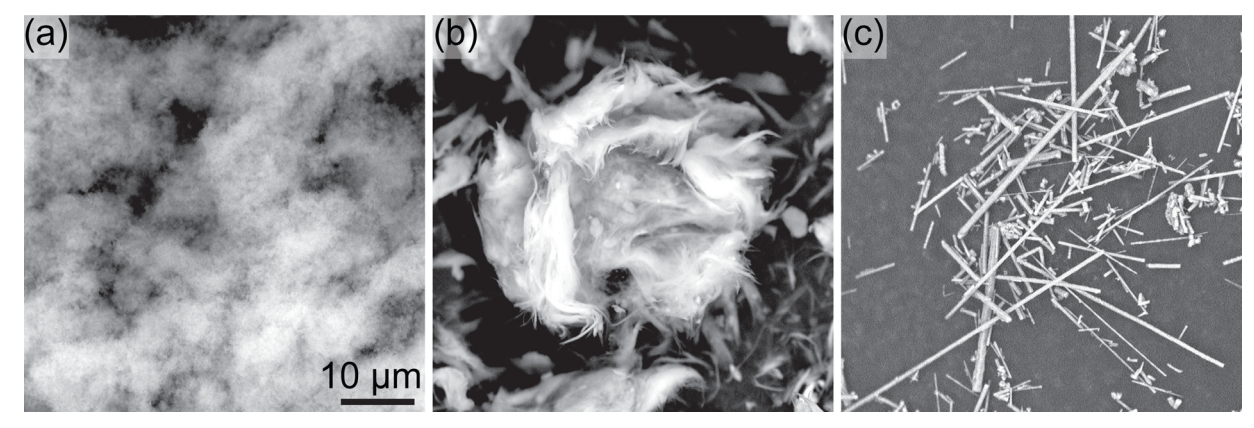


Fig. 2. Scanning electron micrographs showing different morphologies of the as-received filler materials incorporated in this work. (a) fumed silica (FS) particles, (b) nanoclay (NC) platelets and (c) rod-like SiC-whiskers.

Table 1Properties and morphology of individual ink constituents.

Material	Density (g/cc)	Approximate dimensions, thickness \boldsymbol{x} length (μm)	Aspect ratio	Morphology
Epoxy resin Fumed silica (FS)	1.16 2.2	 0.014 × 0.014	~1	liquid Agglomerates of spheroidal nanoparticles
Nanoclay (NC) SiC whiskers	1.6 3.21	0.001 × 0.1 0.65 × 11	100 17	platelets rods

Table 2Composition of inks formulated for direct ink writing.

Filler material	Resin (g)	Curing agent (g)	Filler (wt.%)	Filler (g)	Filler (vol.%)	Density (g/cc)
FS	20	1	10	2.33	5.54	1.232
NC	20	1	10	2.33	7.46	1.237
SiC/FS	20	1	32.4 (SiC), 5.07 (FS)	10.8 (SiC), 1.7 (FS)	15 (SiC), 3.48 (FS)	1.512
SiC/NC	20	1	32.4 (SIC), 5.07 (NC)	10.8 (SiC), 1.7 (NC)	15 (SiC), 4.72 (NC)	1.521

for extrusion. Ink formulations were loaded into 30 cc or 10 cc syringe barrels (Nordson EFD, Westlake, OH) and centrifuged at 3900 rpm for 8 min using a Sorvall™ ST-8 Centrifuge (ThermoFisher Scientific, Waltham, MA) to get rid of any bubbles that may have been introduced during loading, following [4,5]. Tapered metal syringe tips (S-type, GPD, Grand Junction, CO) with different inner diameters (233, 609, 864 and 1041 $\mu m),$ and with the same length were used throughout the study. Tapered nozzles were used because they result in significantly higher flow-rate for a given applied pressure, compared to straight, cylindrical nozzle tips. The layer height and spacing between filaments were specified as 0.6 and 0.85 times the inner diameter of the nozzle, respectively. Rectangular specimens were printed using two different print paths: (1) the longitudinal print path, in which the printed filaments (or roads) were oriented parallel to the length of the specimen (Fig. 1i), and (2) the transverse print path, in which printed filaments were oriented orthogonal to the length of the specimen. Schematic illustrations of the employed print paths are shown in Fig. S1. The desired print paths were defined in G-code using scripts written with Scilab software (Scilab Enterprises, Institut National de Recherche en Informatique et en Automatique, France). All specimens were printed on glass substrates covered with polytetrafluoroethylene (PTFE) coated aluminum foil (Bytac, Saint-Gobain Performance Plastics, Worcester, MA) to avoid permanent adhesion. Samples were printed at print speeds of 10, 20 and 40 mm/s and the extrusion pressure was adjusted to provide a flow-rate to match the print speed in a one to one manner. The extrusion pressure values used for each material system with different nozzle sizes and print speeds are summarized in Table S1. Following printing, samples were pre-cured at 100 °C for 24 h, removed from the substrate, and cured at 220 °C for 2 h on an uncoated glass substrate. Density of printed, cured materials were measured using the Archimedes method.

2.5. Mechanical testing

Printed specimens with nominal dimensions of $40 \times 8 \times 2$ mm were tested in three-point flexure configuration. Top and side surfaces of the transverse specimens were ground flat prior to testing. Tests were carried out at ambient temperature (~21 °C) on an electromechanical load frame (Model 45, MTS Systems Corporation, Eden Prairie, MN, USA) using a 10 kN load cell with a cross-head speed of 0.8 mm/min. All printed specimens were mounted identically in the 3pt-flexural configuration so that the principle stress direction was parallel to the print direction for the longitudinal specimens and transverse to the print direction for the transverse specimens. A span length of 32 mm was used for all specimens. For specimens with strain-to-failure values of ≤ 5 %, the flexural strength was calculated according to ASTM D790 [41]. For specimens with strain-to-failure values greater than 5 %, the

modified stress equation suggested in [42,43] was used to calculate the flexural strength.

2.6. Microscopy

SEM was used to observe select fracture surfaces of tested flexure specimens and to observe the morphology of the individual filler materials prior to ink formulation. Additionally, cross-polarized light microscopy was performed on thin slices of printed specimens using transmitted light to observe birefringence patterns associated with discrete print paths, following [5]. Slices were cut using a low speed sectioning saw (TechCut 4, Allied High Tech Products, Inc. Rancho Dominguez, CA). The surfaces of the cut slices were then polished using aluminum-oxide lapping films (Allied High Tech Products, Inc. Rancho Dominguez, CA). The cut slices had comparable thicknesses ($\sim 0.5 \text{ mm}$ thick) and were inspected with the same light intensity. SEM was performed on a Phenom Desktop SEM (Nanoscience Instruments, Inc, Phoenix, AZ), and cross-polarized light microscopy was performed on a VHX-5000 digital microscope (Keyence Corporation of America, Itasca, IL), equipped with two polarized filters (i.e. polarizer and analyzer). Image analysis was performed using the open source software ImageJ, version 1.52a (http://imagej.nih.gov/ij).

2.7. X-ray scattering

Thin printed samples were characterized using 2D small-angle x-ray scattering (2D-SAXS) and 2D wide-angle X-ray scattering (2D-WAXS) to quantify microstructural ordering of the filler materials as a result of the printing process. SAXS was performed using a Rigaku S-Max 3000 three-pinhole SAXS system, equipped with a rotating anode emitting Xrays with a wavelength of 0.154 nm (Cu Kα). Scattering from a silver behenate standard was used to calibrate a sample-to-detector distance of 1.5 m. Two-dimensional data were collected using a fully integrated 2D multiwire area detector with 2 h exposure time. WAXS was performed using the same equipment with a sample-to-detector distance of 110.0 mm. WAXS two-dimensional diffraction patterns were obtained using an image plate, with an exposure time of 1 h. WAXS data were collected at three different locations on each specimen to obtain an average value of Herman's orientation parameter (f_x) . All WAXS data were analyzed using the SAXSGUI software package to obtain WAXS intensity versus azimuthal angle profiles. For both SAXS and WAXS measurements, the X-ray beam was focused by the three-pinhole system to a size of 0.4 mm in diameter. Samples printed at 20 mm/s were used for all x-ray measurements.

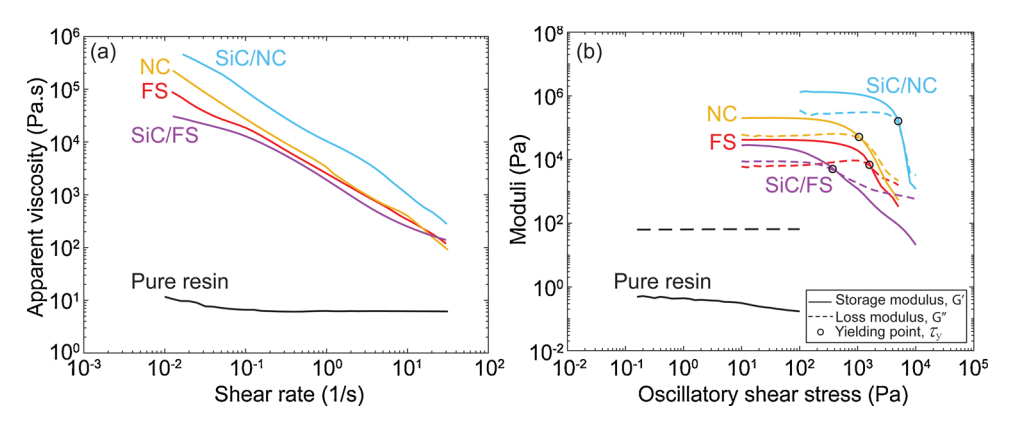


Fig. 3. Rheological behavior of different epoxy-filled systems as it pertains to formulating printable inks for direct ink writing (DIW) process. (a) log-log plots of apparent viscosity as a function of shear rate and (b) the corresponding storage and loss moduli (i.e. viscoelastic properties) versus oscillatory shear stress for the inks shown in (a). The shear yield stress values are measured from the crossover point between the two moduli shown in (b).

3. Results

3.1. Rheological behavior and printing

Pure epoxy resin acts as a Newtonian fluid, with a nearly shear rate-independent viscosity of 10 Pa.s over the shear rate range probed (Fig. 3a). When filler materials are added, the viscosity increases significantly and pronounced shear thinning behavior is observed. At low shear rates ($\sim 10^{-2} \, \text{s}^{-1}$), the viscosity increases in all formulations by four to five orders of magnitude. Both the FS and NC inks display similar apparent viscosities and shear thinning behavior at shear rates greater than $\sim 0.2 \, \text{s}^{-1}$. The shear thinning exponent for these inks, based on a standard power law flow model, ranges from n = 0.03 to 0.25, over the range from 0.01 to 1 s⁻¹. This range indicates good shear thinning behavior and falls within the range of several other reported successful DIW inks [4,5,44,45].

Measurements of storage (G') and loss (G") moduli are plotted in Fig. 3b. For the pure resin, the shear loss modulus is stress-independent (\sim 100 Pa) and is about two orders of magnitude higher than its storage modulus, characteristic of a viscous fluid. As fillers are added to the epoxy resin, both the loss and storage moduli increase, and at low applied stress all inks display solid-like behavior, where the storage modulus is higher than the loss modulus. At higher stresses, the inks yield and flow, indicated by a steep drop in storage modulus. The yield stress approximately corresponds to the crossover point where the storage modulus drops below the loss modulus, indicating a transition from solid-like to liquid-like behavior. The SiC/NC ink exhibits the highest shear yield stress ($\tau_y = 5012 \text{ Pa}$) and the SiC/FS ink exhibits the lowest shear yield stress ($\tau_v = 400 \text{ Pa}$), while the NC and FS inks are more similar in behavior with $\tau_v = 1590$ Pa and 1000 Pa, respectively. Although the range of storage modulus and yield stress values is fairly large, all fall within the range reported for other successful DIW inks [4,5,46,47]. All of the inks were able to be printed out of three distinct nozzle sizes and at three distinct print speeds. Examples of printed specimens are shown in Fig. 1c-i. Moreover, all of the inks were able to successfully produce pore-free, fully dense printed components with the print parameters and pressures chosen. As an example, representative optical micrographs of fracture surfaces are shown in Fig. S3 for longitudinal and transverse flexural specimens printed with the NC ink at varying nozzle sizes and print speeds. In these micrographs, there is no evidence of the original print path, indicating complete coalescence and strong adhesion between adjacent filaments and layers, as reported in

3.2. Mechanical behavior

The flexural modulus and flexural strength of printed composites as a function of nozzle size are shown in Fig. 4. The FS composites have a flexural modulus of 3.1 GPa and flexural strength of 109 MPa, independent of the nozzle size and print direction (Fig. 4a, b). Printed

composites containing anisotropic fillers display an inverse relationship between their flexural strength and stiffness and the nozzle size, when tested along the print direction, while a direct correlation is apparent when tested transverse to the print direction. For example, at the smallest nozzle size, the flexural strength of the NC specimens is 173 MPa along the print directions and 97 MPa transverse to it, while for the largest nozzle size, the flexural strength reduces to 141 MPa along the print directions and increases to 105 MPa transverse to it (Fig. 4d). The same trend is observed in SiC whisker-containing inks, albeit with a greater difference in properties observed along and transverse to the print direction. At the smallest nozzle size, the SiC/NC ink displays a flexural strength of 199 MPa along the print direction and 103 MPa transverse to it.

For the largest nozzle size, these values change to 188 MPa along the print direction and 112 MPa transverse to it. Trends are identical for the SiC/FS ink with strength values being slightly lower along the print direction and slightly higher transverse to it (Fig. 4f). The trends observed for strength are also observed for flexural modulus for each material, with SiC whisker-containing inks displaying the greatest sensitivity to print direction and nozzle size (Fig. 4c,e,g). The flexural modulus and flexural strength of printed composites as a function of print speed are shown in Fig. 5. Again, the FS material exhibits flexural strength and stiffness that is independent of print speed and direction (Fig. 5a, b), whereas specimens with anisotropic filler materials display a pronounced dependence on print speed. Here, the trends are reversed from those observed for nozzle size. For example, the flexural strength of the NC material along the print direction increases with print speed from 132 MPa when printed at 10 mm/s to 159 MPa when printed at 40 mm/s. At the same time, the flexural strength transverse to the print direction decreases from 104 MPa to 96 MPa over the same print speeds (Fig. 5d). As was observed for nozzle size effects, the presence of SiC whiskers increases anisotropy and sensitivity to print speed. At the highest print speed, the SiC/NC composite attains a strength of 216 MPa along the print direction and 93 MPa transverse to it. At the lowest print speed, the strength along the print direction reduces to 180 MPa and the transverse strength increases to 112 MPa. Again, trends are identical for the SiC/FS ink with strength values being slightly lower along the print direction and slightly higher transverse to it (Fig. 5f). The trends observed for strength are also observed for flexural modulus for each material, with SiC whisker-containing inks displaying the greatest sensitivity to print direction and print speed (Fig. 5c,e,g). All flexural properties are summarized in Tables 3 and 4.

3.3. Microscopic characterization

Fig. 6 shows representative optical micrographs for printed composites containing NC in transmitted, cross-polarized light mode. The bottom edges printed slices are aligned parallel to the orientation of the polarizer (at 0 $^{\circ}$ orientation angle). It can be observed that the NC causes distinct birefringence patterns (Fig. 6), with a clear correlation

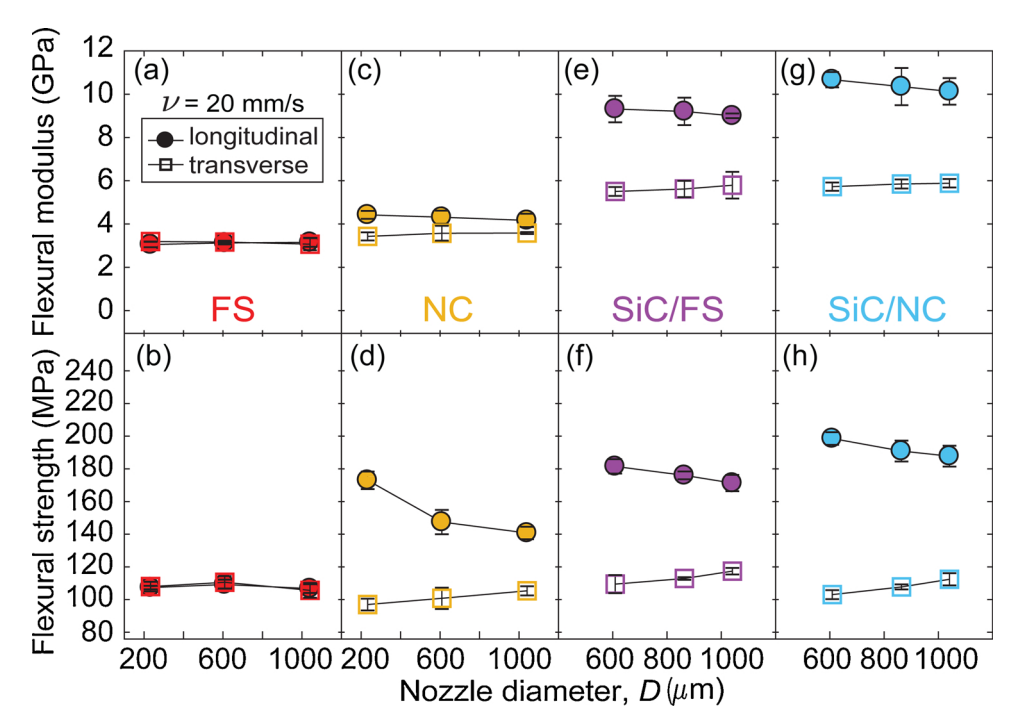


Fig. 4. Flexural properties of longitudinal and transverse specimens as a function of nozzle diameter for epoxy-based composites containing different filler materials. Flexural modulus (top) and flexural strength (bottom) are shown, respectively, for: (a and b) FS, (c and d) NC, (e and f) SiC/FS, and (g and h) SiC/NC composites. All composites were printed at a constant print speed of 20 mm/s.

between the nozzle size and the characteristic size of the birefringence pattern.

The size of the repeat patterns directly corresponds to the size of the nozzle used to print the samples, as indicated on the images by white ovals. In contrast, no birefringence or pattern was observed throughout the bulk of the printed specimens containing FS as previously reported [5], regardless of nozzle diameter (see Fig. S4).

The SiC-based specimens were not transparent enough to be inspected with cross-polarized light microscopy. However, representative SEM micrographs of fracture surfaces for flexure specimens printed with SiC/FS at varying print speeds are shown in Fig. 7. In these micrographs the epoxy matrix is a dull gray while the SiC whiskers are bright white. The longitudinal print path was used for these specimens,

so the print direction is normal to the plane of the image. At a print speed of 10 mm/s, the whiskers appear to be more randomly oriented, as a large number of whiskers can be seen lying predominantly in the plane of the image (Fig. 7a). As print speed increases to 20 mm/s and 40 mm/s, fewer in-plane whiskers are visible, and more whiskers appear as single bright dots, corresponding to an end-on view (Fig. 7b,c). To quantify these qualitative observations, the micrographs were converted to black and white, with white pixels indicating SiC whiskers and black pixels indicating epoxy matrix (Fig. 7d–f). The ratio of white to black pixels provides a measure of the relative area that each phase occupies in the micrograph. For any given whisker, the apparent area is smallest when it is aligned normal to the plane of the image. Therefore, because the volume fraction of whiskers is identical in each of the

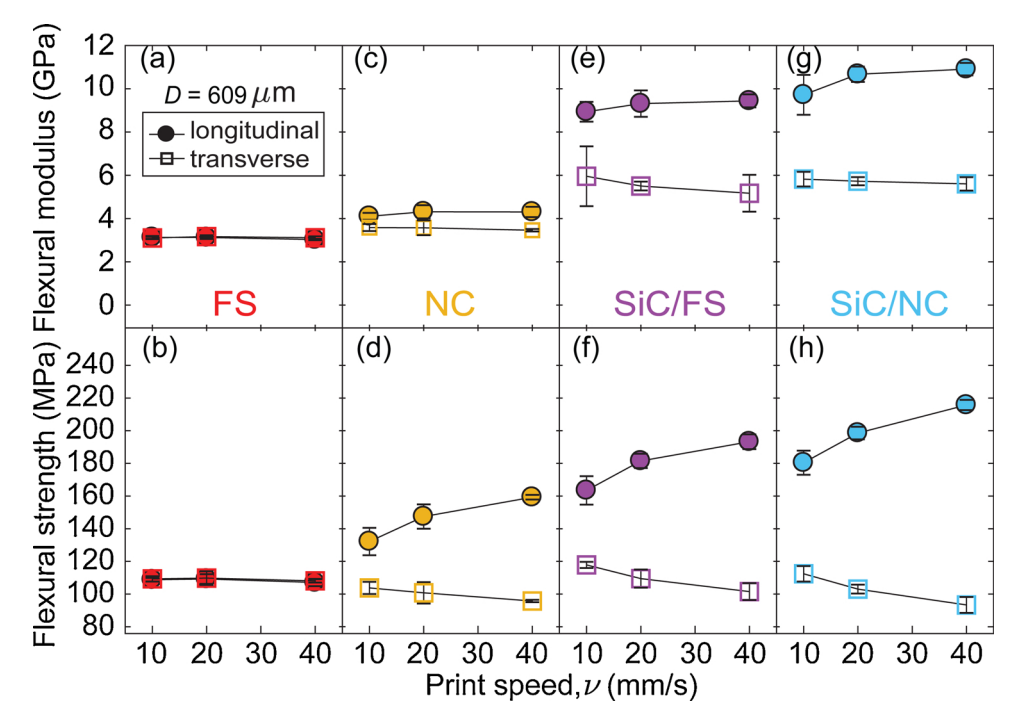


Fig. 5. Flexural properties of longitudinal and transverse specimens as a function of print speed for epoxy-based composites containing different filler materials. Flexural modulus (top) and flexural strength (bottom) are shown, respectively, for: (a and b) FS, (c and d) NC, (e and f) SiC/FS, and (g and h) SiC/NC composites. All samples were printed at a constant deposition nozzle diameter of 609 μm .

Table 3 Flexural properties of FS- and NC-based 3D-printed specimens.

Filler material	Nozzle size (µm)	Print speed (mm/s)	Print path*	Flexural modulus (GPa)	Flexural strength (MPa)	Strain-to-failure (%)	Number of specimens
FS	233	20	L	3.05 ± 0.13	107.3 ± 1.09	4.99 ± 0.00	4
			T	3.19 ± 0.01	107.9 ± 2.95	4.66 ± 0.30	4
	609	20	L	3.13 ± 0.07	109.2 ± 2.98	4.99 ± 0.01	6
			T	3.17 ± 0.06	110.6 ± 3.76	4.65 ± 0.29	4
	1041	20	L	3.16 ± 0.21	106.7 ± 2.68	4.98 ± 0.03	4
			T	3.07 ± 0.28	105.6 ± 4.54	4.61 ± 0.05	4
	609	10	L	3.13 ± 0.07	108.8 ± 1.12	5.00 ± 0.00	4
			T	3.10 ± 0.06	109.3 ± 1.64	4.60 ± 0.09	4
	609	40	L	3.03 ± 0.03	107.1 ± 2.23	4.97 ± 0.12	4
			T	3.11 ± 0.07	108.1 ± 1.01	4.47 ± 0.10	4
NC	233	20	L	4.42 ± 0.18	173.0 ± 5.38	5.26 ± 0.11	4
			T	3.43 ± 0.19	97.0 ± 3.59	3.32 ± 0.26	5
	609	20	L	4.32 ± 0.30	147.4 ± 7.45	4.64 ± 0.19	5
			T	3.57 ± 0.34	100.8 ± 6.54	3.27 ± 0.14	6
	1041	20	L	4.17 ± 0.31	140.7 ± 3.85	4.45 ± 0.26	5
			T	3.58 ± 0.05	105.4 ± 2.81	3.69 ± 0.19	4
	609	10	L	4.11 ± 0.16	132.2 ± 8.39	4.41 ± 0.52	5
			T	3.59 ± 0.16	103.8 ± 3.72	3.54 ± 0.19	4
	609	40	L	4.31 ± 0.24	159.3 ± 1.43	5.06 ± 0.08	4
			T	3.46 ± 0.06	95.7 ± 0.73	3.15 ± 0.06	4

^{*} L: longitudinal; T: transverse.

samples, comparison of the ratios of white-to-black pixels provides an indication of the relative alignment of the whiskers between samples, with a lower ratio indicating greater alignment. The white-to-black ratio varies from 0.15 to 0.11 to 0.07 for print speeds of 10, 20, and 40 mm/s, respectively. We note that this approach does not result in a direct measure of whisker orientation.

3.4. X-ray scattering

SAXS 2D patterns of the FS material system for the three deposition nozzle diameters show symmetric, isotropic scattering (Fig. 8a–c). In contrast, 2D scattering patterns from the NC material (Fig. 8d–f) show anisotropic scattering along the vertical axis, indicating orientation along the horizontal axis (corresponding to the print direction) from all nozzle diameters. 2D WAXS scattering patterns were also collected for the same samples (Fig. 9). No orientation is observed in the 2D WAXS patterns from the FS printed specimens (Fig. 9a–c), regardless of nozzle size, whereas high intensity scattering along the vertical axis at a

scattering angle of 0.51 Å $^{-1}$ is visible in the scattering patterns from the NC specimens all nozzle diameters (Fig. 9d–f). The sharp, anisotropic scattering observed in the scattering patterns of the NC samples occurs at a scattering angle of 0.51 Å $^{-1}$ (7° 20), which is consistent with a dspacing of 1.2 nm between the silicate platelets in the tactoids of Garamite nanoclay [48]. The degree of NC orientation was quantified using Herman's orientation factor. The two intensity maxima of background-corrected tactoid scattering intensity (0.50 Å $^{-1}$ < q < 0.55 Å $^{-1}$) as a function of azimuthal angle were fit using Gaussian functions. Individual Gaussian fits were then shifted horizontally along the azimuthal angle until centered about 0° (Fig. S5) and then used to determine Herman's orientation factor, f_r , using Eqs. 1 and 2:

$$f_{x} = 1 - 3\overline{\sin^{2}\delta} \tag{1}$$

$$\overline{\sin^2 \delta} = \frac{\int_0^{\pi/2} I(\delta) \sin^2 \delta \cos \delta d\delta}{\int_0^{\pi/2} I(\delta) \cos \delta d\delta}$$
(2)

Table 4 Flexural properties of SiC-based 3D-printed specimens.

Filler material	Nozzle size (µm)	Print speed (mm/s)	Print path*	Flexural modulus (GPa)	Flexural strength (MPa)	Strain-to-failure (%)	Number of specimens
SiC/FS	609	20	L	9.31 ± 0.61	181.5 ± 4.40	3.39 ± 0.11	6
			T	5.51 ± 0.21	109.5 ± 5.55	3.03 ± 0.20	4
	864	20	L	9.20 ± 0.63	176.0 ± 2.39	3.35 ± 0.05	4
			T	5.62 ± 0.38	112.9 ± 0.80	3.17 ± 0.13	4
	1041	20	L	9.00 ± 0.11	171.3 ± 4.99	3.26 ± 0.19	5
			T	5.79 ± 0.62	117.4 ± 1.99	3.20 ± 0.15	4
	609	10	L	8.94 ± 0.46	163.5 ± 8.71	3.33 ± 0.40	6
			T	5.96 ± 1.38	117.8 ± 1.90	3.20 ± 0.12	4
	609	40	L	9.44 ± 0.30	193.3 ± 4.51	3.42 ± 0.25	4
			T	5.17 ± 0.85	101.5 ± 5.18	2.96 ± 0.10	4
SiC/NC	609	20	L	10.67 ± 0.36	198.6 ± 3.87	2.51 ± 0.05	4
			T	5.73 ± 0.19	103.0 ± 2.75	2.15 ± 0.12	6
	864	20	L	10.35 ± 0.86	190.9 ± 6.40	2.51 ± 0.29	4
			T	5.85 ± 0.21	107.7 ± 1.54	2.17 ± 0.05	4
	1041	20	L	10.13 ± 0.61	187.8 ± 6.40	2.48 ± 0.13	5
			T	5.89 ± 0.20	112.4 ± 3.71	2.40 ± 0.19	4
	609	10	L	9.72 ± 0.92	180.4 ± 7.40	2.40 ± 0.39	4
			T	5.82 ± 0.34	112.4 ± 4.74	2.37 ± 0.22	5
	609	40	L	10.91 ± 0.29	215.7 ± 3.13	2.84 ± 0.20	4
			T	5.61 ± 0.31	93.3 ± 4.84	2.02 ± 0.17	4

^{*} L: longitudinal; T: transverse.

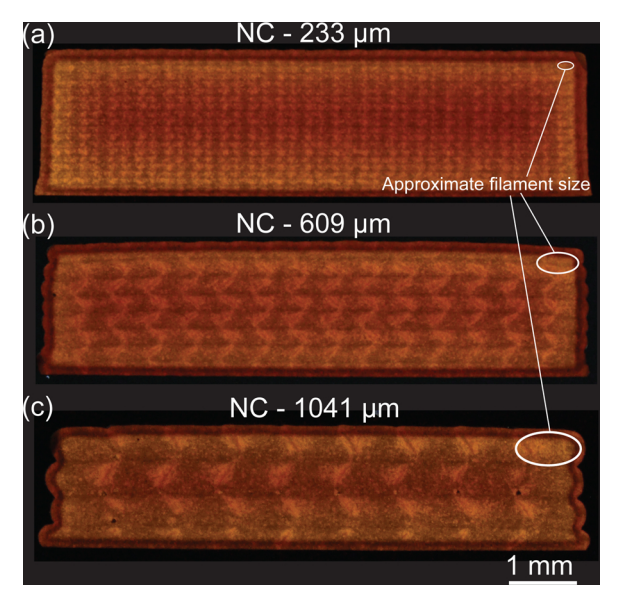


Fig. 6. Representative optical transmitted light micrographs of polished thin slices (<1 mm thick) cut from printed specimens containing NC filler, observed using crossed polarizers. Specimens printed with nozzle diameters of (a) 233 μm , (b) 609 μm and (c) 1041 μm . These samples show strong periodic variations in birefringence that have length scales comparable to the diameter of the nozzle used for printing. The axis of the printed filaments is normal to the plane of the image.

where δ is the azimuthal angle in radians [49]. As shown in Table 5, NC platelets become more oriented as nozzle size decreases. This quantitative analysis corroborates the mechanical and cross-polarized light

observations for both FS and NC material systems.

4. Analysis and discussion

4.1. Rheology of composite inks

Although both fumed silica and nanoclay are strong rheology modifiers in the epoxy resin, and shear thinning behavior at 5 wt.% and 10 wt.% loading is similar for each material (Figs. S2 and 3), FS and NC impart notably different storage modulus and yield stress to the epoxy resin, particularly in the presence of an additional filler material, such as SiC whiskers. For example, the FS ink possesses a higher yield stress than the NC ink, which suggests that that fumed silica may be a better viscosifier to use when formulating a composite ink. However, when combined with SiC whiskers to make the SiC/NC and SiC/FS inks, the FS results in a significantly lower yield stress and storage modulus compared to the ink that utilizes NC with SiC whiskers. This may be related to potential interactions between the FS and SiC, different length scales of the networks that FS and NC form relative to the size of SiC whiskers, or how each of the filler materials forms a network within the resin. These observations are the subject of ongoing study.

4.2. Anisotropy master curves

In the course of this study, we have varied nozzle size and print speed to investigate how such parameters influence anisotropy in printed composites. The results clearly indicate that particle alignment and mechanical anisotropy are influenced by both of these parameters. However, because the flow rate of the ink was matched to the translation speed of the print head, and the layer height was fixed at 60 % of the nozzle diameter, changes to nozzle size were accompanied by

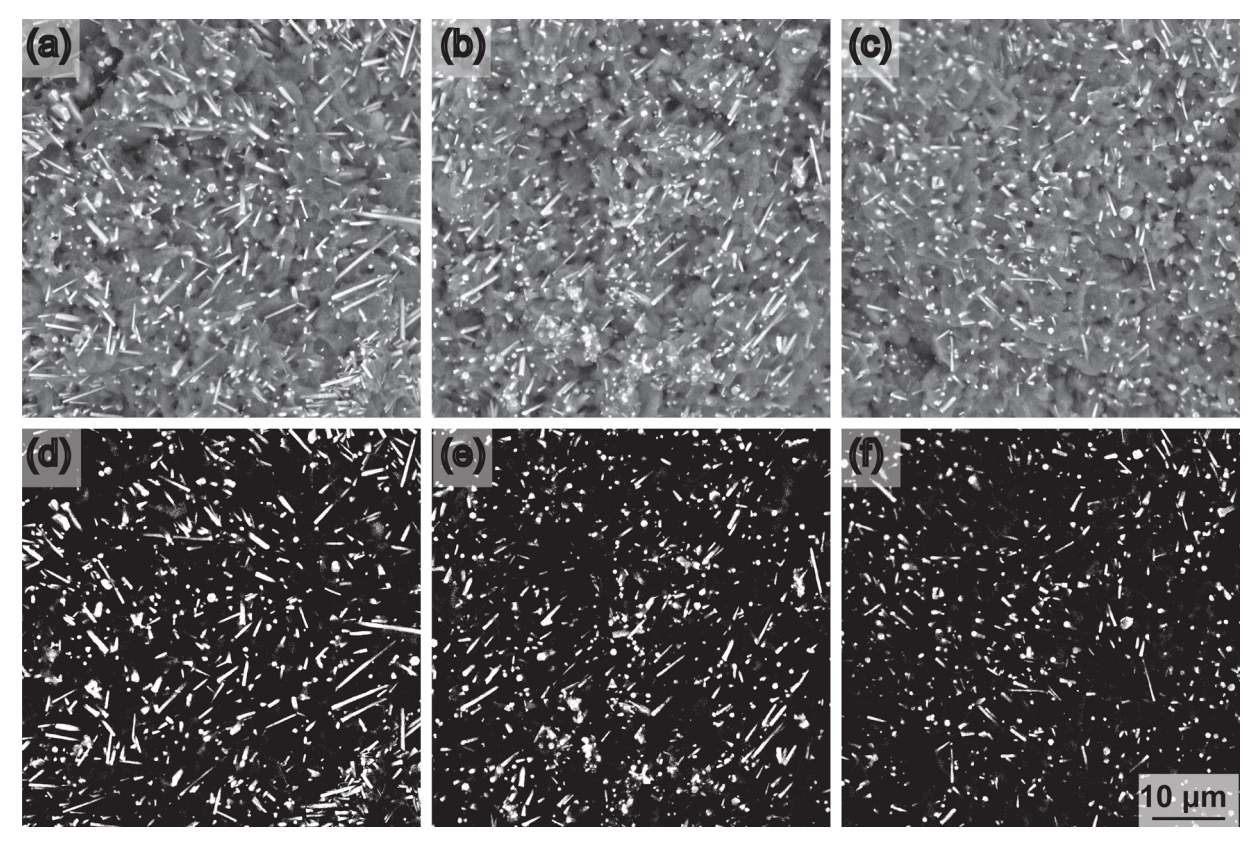


Fig. 7. Representative SEM micrographs of selected fracture surfaces for longitudinal flexural specimens with SiC/FS ink at varying print speeds: (a) 10, (b) 20 and (c) 40 mm/s. (d – f) Binary images of corresponding SEM micrographs analyzed with ImageJ to enable quantitative correlation between print speed and whisker alignment. White pixels indicate SiC-whiskers and black pixels indicate epoxy matrix. The print direction is normal to the plane of the image, thus SiC whiskers are observed to become more oriented (indicated by fewer in-plane whiskers) in the print direction as print speed increases (from left-to-right).

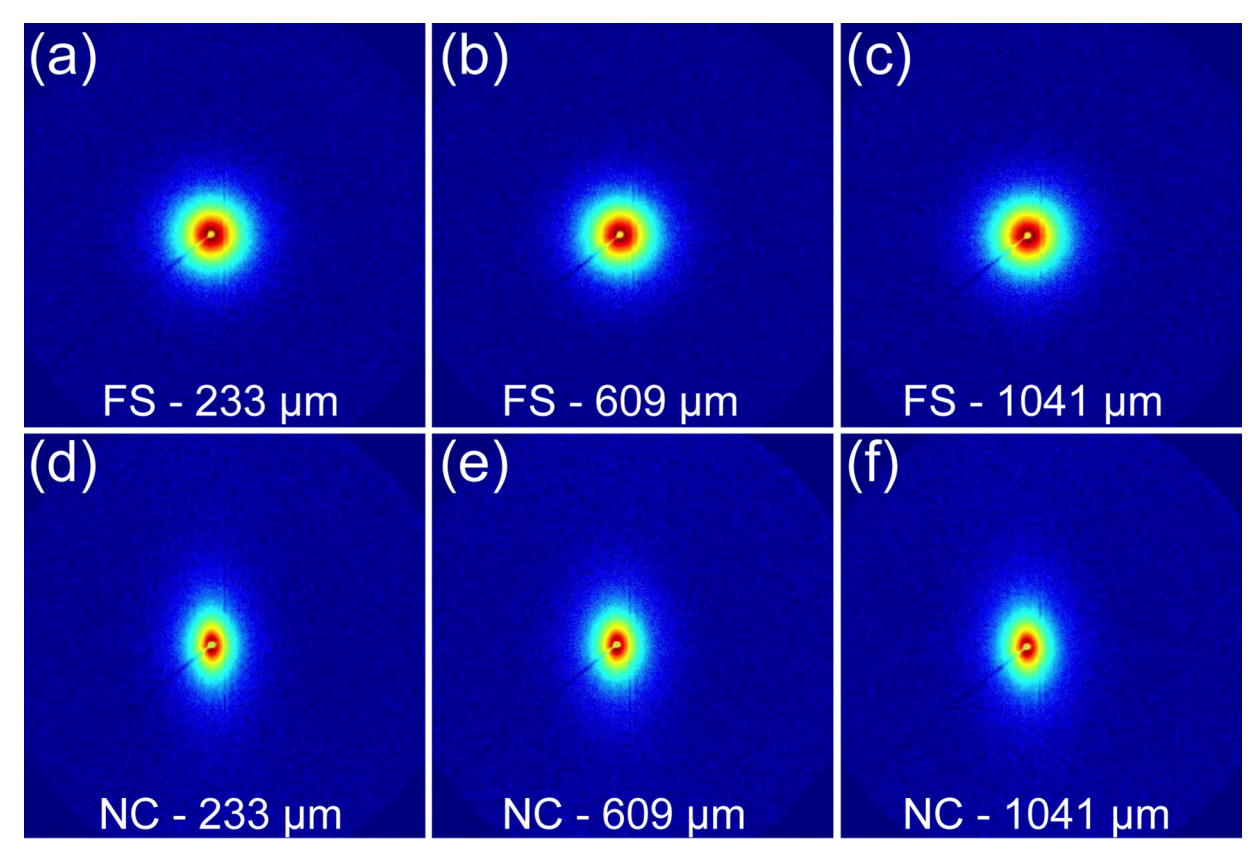


Fig. 8. (a-c) SAXS 2D patterns for printed FS composites and (d-f) NC composites with nozzle diameters of 233 μ m, 609 μ m, and 1041 μ m, in which the print direction is oriented along the horizontal axis.

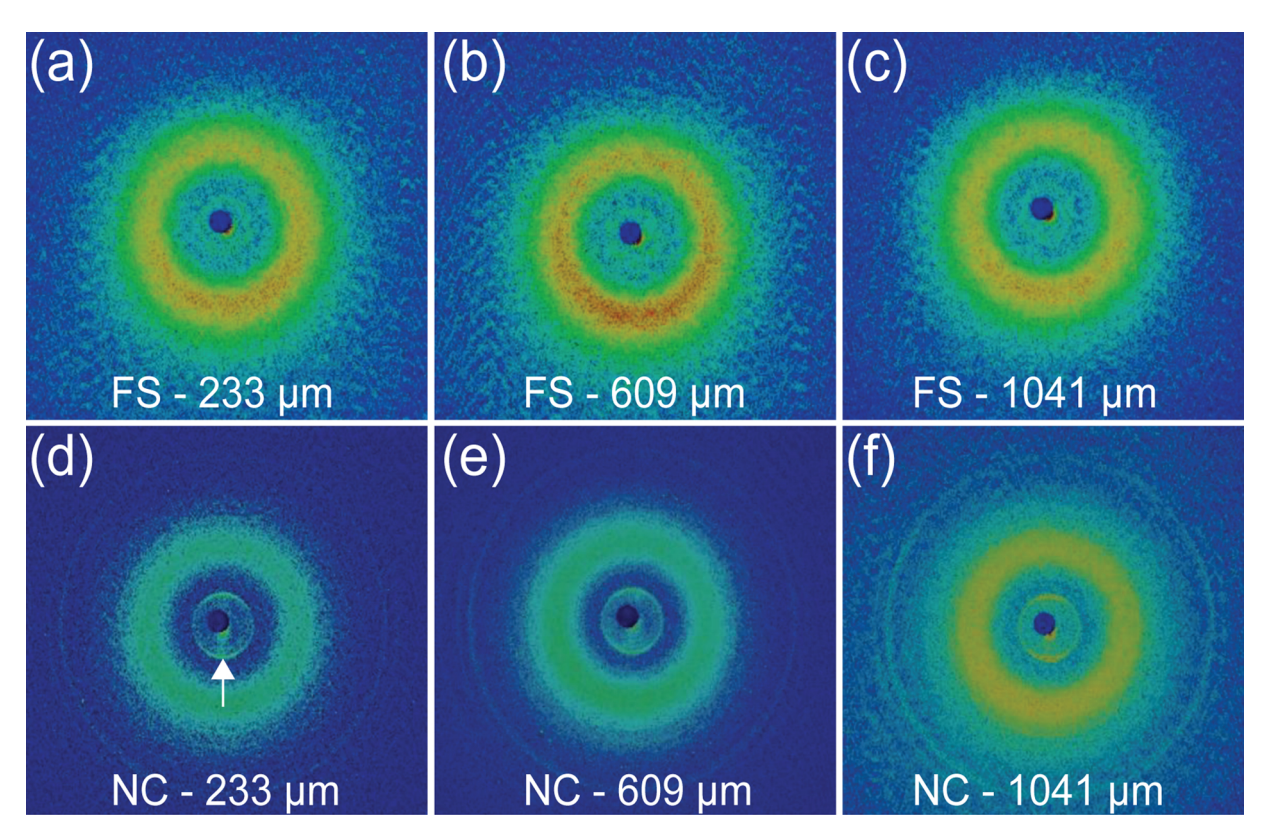


Fig. 9. (a–c) WAXS 2D patterns for printed FS composites and (d-f) NC composites with nozzle diameters of 233 μ m, 609 μ m, and 1041 μ m, in which the print direction is along the horizontal axis. Scattering at 0.51 Å⁻¹ is denoted by an arrow in (d).

Table 5 Herman's orientation factor, f_v , in NC-containing composites.

Nozzle size (µm)	233	609	1041
f_x	0.65 ± 0.03	0.56 ± 0.04	0.51 ± 0.03

changes to the shear rate in the fluid between the nozzle and the substrate and these tests were unable to unambiguously probe the effects of draw ratio in isolation. The presence of this shear field between the translating nozzle and the stationary substrate is a necessary feature of material extrusion AM, which would appear to preclude clean studies of draw ratio in AM processes without changing the diameter of the reservoir. With this in mind, the two data sets generated in this study can be compared by defining a normalized translation rate that is proportional to the shear rate between the nozzle and substrate:

$$v^* \equiv \frac{v}{D} \propto \frac{v}{h} \tag{3}$$

where ν is the print speed, D is the diameter of the deposition nozzle, and h is the layer height. The physical interpretation of this quantity is unambiguous, regardless of the properties of the fluid or the specific geometry of the nozzle and it enables direct comparisons between different combinations of nozzle size and translation rate.

In addition, we define an anisotropy factor as the ratio of the longitudinal to transverse property of printed composites:

$$\psi \equiv \frac{M_L}{M_T} \tag{4}$$

where ψ is the anisotropy factor, M is either the strength or modulus, and the subscripts L and T indicate the longitudinal and transverse properties, respectively. Using these definitions, all of the mechanical test data for a given material system collapse onto one curve that

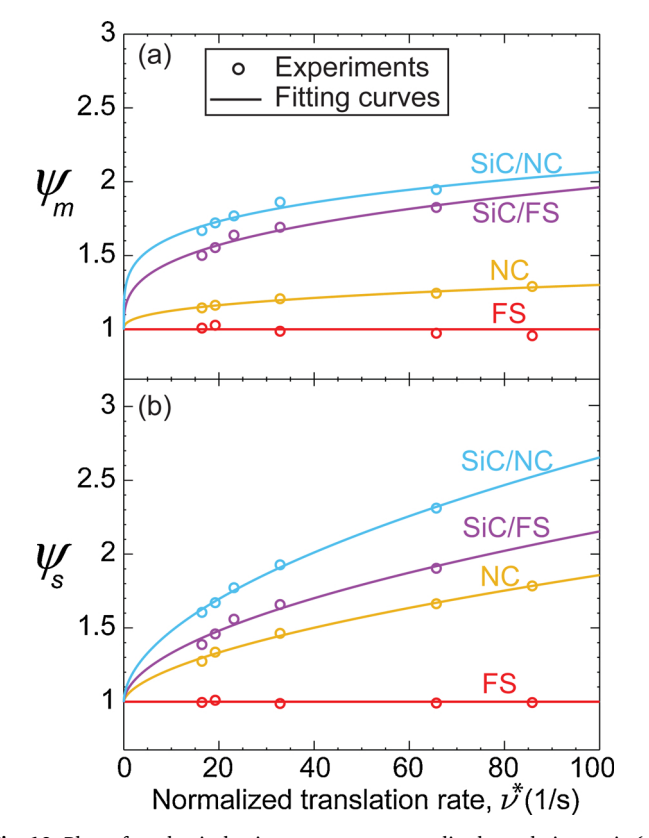


Fig. 10. Plots of mechanical anisotropy versus normalized translation rat in (a) modulus and (b) strength for all the samples tested. Solid lines are the fit of the power-law model given in Eq. 5.

Table 6Fitting parameters for power law anisotropy model.

	Fitting parameters					
	Modulus		Strength			
Filler material	A	b	A	b		
FS	0	1	0	1		
NC	0.05	0.38	0.06	0.60		
SiC/FS	0.22	0.32	0.10	0.54		
SiC/NC	0.36	0.23	0.14	0.54		

indicates a single functional relationship between normalized translation rate and mechanical anisotropy (Fig. 10). Plotted in this manner, we see that the anisotropy factor approaches a value of unity as the normalized translation rate approaches zero, indicating that the printed composites approach isotropic behavior as the print speed approaches zero or as the nozzle size approaches $+\infty$. Based on this observation, a two-parameter power-law model is proposed to fit the data:

$$\psi = 1 + A(v^*)^b \tag{5}$$

where A and b are the fitting parameters. Table 6 lists the values of A and b computed for each material system, for both modulus and strength data, computed using non-linear regression. Model predictions are also plotted with the data points in Fig. 10.

These master curves and power law model allow one to make direct comparisons of a wide range of printing tests to provide insight into the phenomena that govern anisotropy in printed composite materials. We anticipate that every combination of filler material and resin will have a characteristic master anisotropy curve that depends on the viscosity of the resin, the size and morphology of the filler material, and the geometry of the deposition nozzle. Thus, for a given printing system and material, a select few mechanical tests can enable predictions of mechanical properties and anisotropy over a broad range of printing parameters. This can be very important for enabling more rigorous engineering design of 3D-printed composite materials and may even provide a pathway to spatially program mechanical properties using only print parameters. It is important to note that the upper limit of the anisotropy factor is dictated by the properties that would result from perfectly aligned fillers, above which the anisotropy factor would adopt a constant value. This limiting behavior is not captured in the model at present.

4.3. Interaction between fillers

Experimental observations showed that the FS-based composite exhibits mechanical behavior that is independent of both print direction and normalized translation rate. Therefore, the increase in mechanical properties that is observed in the SiC/FS ink with increasing normalized translation rate is assumed to result entirely from the reinforcing effect of the SiC whiskers as they become more oriented along the print direction. However, when considering the SiC/NC system, both the SiC whiskers and the NC are expected to contribute to the dependence of the mechanical properties on the normalized translation rate. Indeed, each filler material individually displays strong sensitivity to deposition rate. If both species of filler behave independently in the epoxy matrix, then a synergistic effect may be expected. That is, if the epoxy and clay are thought of together as the matrix, and the SiC whiskers as the reinforcing species, then an increase in normalized translation rate would result in strengthening of the matrix alone - from increased alignment of the clay particles, leading to higher composite strength - and strengthening of the composite through increased alignment of the SiC whiskers. If that description is accurate, then one would expect to see significantly different behavior between the SiC/FS and SiC/NC inks. Interestingly, while the SiC/NC composite is stiffer and stronger along

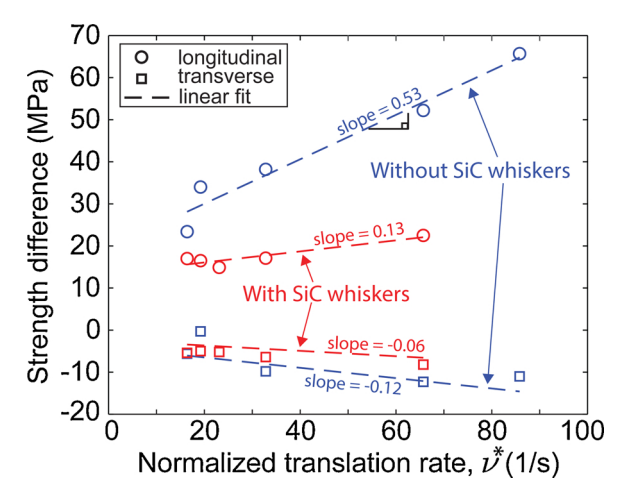


Fig. 11. The difference in strength between the NC and FS composites (blue), and between the SiC/NC and SiC/FS (red) composites as a function of normalized translation rate. Dashed lines represent the linear regression of each data set. Plotted in this manner, the data suggest that NC is less influenced by normalized translation rate in the presence of SiC whiskers.

the print direction than the SiC/FS composite, the difference is small compared to the difference in strength between the NC- and FS-only composites at comparable print parameters. To highlight this observation, we have plotted the difference in strength between the NC and FS composites, and between the SiC/NC and SiC/FS composites as a function of normalized translation rate in Fig. 11. Along the print direction, the NC composite is 20-30 MPa stronger than the FS composite at low normalized translation rate, and 60-70 MPa stronger at high normalized translation rate. Conversely, the SiC/NC composite is only 10-20 MPa stronger than the SiC/FS composite across the entire range of normalized translation rates investigated. One possible explanation for this observation is that the presence of SiC whiskers frustrates the orientation of the clay platelets during the deposition process by altering the local shear rate and stress state in the vicinity of the whiskers, thereby diminishing the propensity of the smaller clay platelets to align along the print direction. This phenomenon could have important implications for the design of optimal composite feedstocks for material extrusion AM, and further study is warranted.

5. Summary and conclusions

In this work we have investigated the effects of filler morphology, nozzle size, and print speed on the mechanical anisotropy in 3D printed epoxy composites fabricated via DIW. We have also characterized the effects of different filler materials on the rheology of an epoxy resin to formulate printable composite inks for DIW. The key results of this work can be summarized as follows:

- Printed epoxy/FS composites were shown to exhibit mechanical behavior that is independent of nozzle size, print speed, and print path, with flexural strength and modulus of 107 MPa and 3.1 GPa, respectively.
- SiC whisker-reinforced printed composites display flexural strength values up to 215 MPa along the print direction. To the authors' knowledge, this is currently the highest reported flexural strength for a 3D-printed whisker-reinforced polymer composite.
- X-ray scattering measurements confirmed the alignment and dependence on print parameters of nanoclay platelets in printed composites.
- The mechanical properties of printed composites containing highaspect-ratio fillers display pronounced dependence on both nozzle size and print speed. For the resin and filler combinations utilized in this study, we have found that a power law describes the

relationship between mechanical anisotropy and normalized translation rate.

 Both nanoclay and fumed silica are highly effective at imparting shear thinning and yield stress behavior to epoxy resin, but nanoclay appears to be more effective for formulating inks with multiple filler materials. However, in the printed composites, the presence of larger filler materials may disrupt the alignment of clay platelets during the deposition process.

Anisotropy in printed components is a critical issue that complicates the straightforward design of AM components. We believe this study represents an important step towards enabling the application of rigorous engineering design principles to AM component design. In addition, the study highlights the possibility of additively manufacturing complex components with programmed anisotropy simply through the systematic variation of print parameters and ink constituents.

Declaration of Competing Interest

The authors have no conflicts of interest associated with this work.

Acknowledgments

This research was supported through funding from NSF under grant no. CMMI-1825815, and Honeywell Federal Manufacturing and Technologies through Contract DE-NA0002839, administrated by Dr. Jamie Messman, Mr. Steven Patterson, and Dr. Eric Eastwood. The authors would also like to thank Prof. Michael Kilbey for helpful discussion and Mr. James W. Kemp for assistance with SEM imaging. BGC and RCP would like to acknowledge partial support from the Tennessee Higher Education Commission Center for Materials Processing. SJT acknowledges financial support from Doctoral Scholars program of the Virginia Tech Institute for Critical Technology and Applied Science (ICTAS). SiC whiskers were generously provided by Mr. Kevin Fox at Haydale Technologies, Inc.

Appendix A. Supplementary data

Supplementary material related to this article can be found, in the online version, at doi:https://doi.org/10.1016/j.addma.2020.101385.

References

- J.W. Stansbury, M.J. Idacavage, 3D printing with polymers: challenges among expanding options and opportunities, Dent. Mater. 32 (1) (2016) 54–64.
- [2] X. Wang, et al., 3D printing of polymer matrix composites: a review and prospective, Compos. Part B: Eng. 110 (2017) 442–458.
- [3] A. Shen, et al., 3D printing of polymer-bonded magnets from highly concentrated, plate-like particle suspensions, Mater. Des. 183 (2019) 108133.
- [4] B.G. Compton, J.A. Lewis, 3D-printing of lightweight cellular composites, Adv. Mater. 26 (34) (2014) 5930–5935.
- [5] N.S. Hmeidat, J.W. Kemp, B.G. Compton, High-strength epoxy nanocomposites for 3D printing, Compos. Sci. Technol. 160 (2018) 9–20.
- [6] D.A. Rau, et al., Ultraviolet-assisted direct ink write to additively manufacture all-aromatic polyimides, ACS Appl. Mater. Interfaces 10 (41) (2018) 34828–34833.
- [7] J.P. Bell, Flow orientation of short fiber composites, J. Compos. Mater. 3 (2) (1969) 244–253.
- [8] M. Farkash, D. Brandon, Whisker alignment by slip extrusion, Mater. Sci. Eng. A 177 (1) (1994) 269–275.
- [9] G. Ausias, J.-F. Agassant, M. Vincent, Flow and fiber orientation calculations in reinforced thermoplastic extruded tubes, Int. Polym. Process. 9 (1) (1994) 51–59.
- [10] L.A. Goettler, Mechanical property enhancement in short-fiber composites through the control of fiber orientation during fabrication, Polym. Compos. 5 (1) (1984) 60–71.
- [11] K.N. Murty, G. Modlen, Experimental characterization of the alignment of short fibers during flow, Polym. Eng. Sci. 17 (12) (1977) 848–853.
- [12] D. Pope, A. Keller, Alignment of macromolecules in solution by elongational flow; a study of the effect of pure shear in a four roll mill, Colloid Polym. Sci. 255 (7) (1977) 633–643.
- [13] F. Wittemann, et al., Injection molding simulation of short fiber reinforced thermosets with anisotropic and non-Newtonian flow behavior, Compos. Part A: Appl. Sci. Manuf. (2019) 105476.

- [14] C.E. Duty, et al., Structure and mechanical behavior of big area additive manufacturing (BAAM) materials, Rapid Prototyp. J. 23 (1) (2017) 181–189.
- [15] H.L. Tekinalp, et al., Highly oriented carbon fiber-polymer composites via additive manufacturing, Compos. Sci. Technol. 105 (2014) 144–150.
- [16] H. Pierson, et al., Mechanical properties of printed epoxy-carbon Fiber composites, Exp. Mech. (2019) 1–15.
- [17] J.P. Lewicki, et al., 3D-printing of meso-structurally ordered carbon fiber/polymer composites with unprecedented orthotropic physical properties, Sci. Rep. 7 (2017) 43401.
- [18] P. Calvert, T.L. Lin, H. Martin, Extrusion freeform fabrication of chopped-fibre reinforced composites, High Perform. Polym. 9 (4) (1997) 449–456.
- [19] J. Peng, T.L. Lin, P. Calvert, Orientation effects in freeformed short-fiber composites, Compos. Part A: Appl. Sci. Manuf. 30 (2) (1999) 133–138.
- [20] Y. Kanarska, et al., Fiber motion in highly confined flows of carbon fiber and non-Newtonian polymer, J. Nonnewton. Fluid Mech. 265 (2019) 41–52.
- [21] M.K. Agarwala, et al., Structural quality of parts processed by fused deposition, Rapid Prototyp. J. 2 (4) (1996) 4–19.
- [22] N. Nawafleh, E. Celik, Additive manufacturing of short fiber reinforced thermoset composites with unprecedented mechanical performance, Addit. Manuf. 33 (2020) 101110
- [23] B.G. Compton, et al., Electrical and mechanical properties of 3D-printed graphenereinforced epoxy, JOM 70 (3) (2018) 292–297.
- [24] D.S. Melchert, et al., Flexible conductive composites with programmed electrical anisotropy using acoustophoresis, Adv. Mater. Technol. (2019) 1900586.
- [25] M. Spoerk, et al., Anisotropic properties of oriented short carbon fibre filled polypropylene parts fabricated by extrusion-based additive manufacturing, Compos. Part A: Appl. Sci. Manuf. 113 (2018) 95–104.
- [26] J.R. Raney, et al., Rotational 3D printing of damage-tolerant composites with programmable mechanics, Proc. Natl. Acad. Sci. 115 (6) (2018) 1198–1203.
- [27] D. Kokkinis, M. Schaffner, A.R. Studart, Multimaterial magnetically assisted 3D printing of composite materials. Nat. Commun. 6 (2015) 8643.
- [28] R.R. Collino, et al., Acoustic field controlled patterning and assembly of anisotropic particles, Extreme Mech. Lett. 5 (2015) 37–46.
- [29] R.R. Collino, et al., Deposition of ordered two-phase materials using microfluidic print nozzles with acoustic focusing, Extreme Mech. Lett. 8 (2016) 96–106.
- [30] A.S. Gladman, et al., Biomimetic 4D printing, Nat. Mater. 15 (4) (2016) 413.
- [31] G.B. Jeffery, The motion of ellipsoidal particles immersed in a viscous fluid, Proc. R. Soc. London, Ser. A 102 (715) (1922) 161–179.
- [32] F. Folgar, C.L. Tucker III, Orientation behavior of fibers in concentrated

- suspensions, J. Reinf. Plast. Compos. 3 (2) (1984) 98-119.
- [33] B. Trevelyan, S. Mason, Particle motions in sheared suspensions. I. Rotations, J. Colloid Sci. 6 (4) (1951) 354–367.
- [34] S.G. Advani, C.L. Tucker III, The use of tensors to describe and predict fiber orientation in short fiber composites, J. Rheol. 31 (8) (1987) 751–784.
- [35] L.A. Goettler, Molding of Oriented Short Fiber Composites. III. Rate Effects on Fiber Alignment in Convergent Channels, Monsanto Research Corp St Louis Mo, 1974.
- [36] H. Watanabe, T. Kimura, T. Yamaguchi, Particle orientation during tape casting in the fabrication of grain-oriented bismuth titanate, J. Am. Ceram. Soc. 72 (2) (1989) 289–293
- [37] M. Wu, G.L. Messing, Fabrication of oriented SiC-whisker-reinforced mullite matrix composites by tape casting, J. Am. Ceram. Soc. 77 (10) (1994) 2586–2592.
- [38] G. Galgali, S. Agarwal, A. Lele, Effect of clay orientation on the tensile modulus of polypropylene–nanoclay composites, Polymer 45 (17) (2004) 6059–6069.
- [39] S.H. Ahn, et al., Anisotropic material properties of fused deposition modeling ABS, Rapid Prototyp. J. 8 (4) (2002) 248–257.
- [40] A. Bellini, S. Güçeri, Mechanical characterization of parts fabricated using fused deposition modeling, Rapid Prototyp. J. 9 (4) (2003) 252–264.
- [41] C. ASTM, ASTM Standards, American Society for Testing Materials, Philadelphia,
- [42] M. Giannotti, et al., Role of intrinsic flaws upon flexural behaviour of a thermoplastic modified epoxy resin, Polym. Test. 22 (4) (2003) 429–437.
- [43] A. Nohales, et al., Morphology, flexural, and thermal properties of sepiolite modified epoxy resins with different curing agents, Eur. Polym. J. 42 (11) (2006) 3003–3101
- [44] K.B. Manning, et al., Self assembly–assisted additive manufacturing: direct ink write 3D printing of epoxy–amine thermosets, Macromol. Mater. Eng. 304 (3) (2019) 1200511
- [45] L. Friedrich, et al., Acoustic control of microstructures during direct ink writing of two-phase materials, Sens. Actuators A: Phys. 268 (2017) 213–221.
- [46] G. Siqueira, et al., Cellulose nanocrystal inks for 3D printing of textured cellular architectures, Adv. Funct. Mater. 27 (12) (2017) 1604619.
- [47] T.S. Wei, et al., 3D printing of customized li-ion batteries with thick electrodes, Adv. Mater. 30 (16) (2018) 1703027.
- [48] S. Gurusideswar, R. Velmurugan, N.K. Gupta, Study of rate dependent behavior of glass/epoxy composites with nanofillers using non-contact strain measurement, Int. J. Impact Eng. 110 (2017) 324–337.
- [49] J.K.S. Warrier, V.G. Munshi, P.K. Chidambareswaran, Calculating Herman's orientation factor, Text. Res. J. 57 (9) (1987) 554–555.